Parametrical Modeling and Design Optimization of Blood Plasma Separation Device with Microchannel Mechanism

Xiangdong Xue[1], Mayur K Patel[1], Maïwenn Kersaudy-Kerhoas[2], Chris Bailey[1], Marc P.Y. Desmulliez[2]
[1] School of Computing and Mathematical Sciences, University of Greenwich, London SE10 9LS, UK
[2] MIcroSystems Engineering Centre (MISEC), School of Engineering & Physical Sciences, Heriot-Watt University, Edinburgh, EH14 4AS, UK

Abstract

This paper presents an analysis of biofluid behavior in a T-shaped microchannel device and a design optimization for improved biofluid performance in terms of particle liquid separation. The biofluid is modeled with single phase shear rate non-Newtonian flow with blood property. The separation of red blood cell from plasma is evident based on biofluid distribution in the microchannels against various relevant effects and findings, including Zweifach-Fung bifurcation law, Fahraeus effect, Fahraeus-Lindqvist effect and cell-free phenomenon. The modeling with the initial device shows that this T-microchannel device can separate red blood cell from plasma but the separation efficiency among different bifurcations varies largely. In accordance with the imbalanced performance, a design optimization is conducted. This includes implementing a series of simulations to investigate the effect of the lengths of the main and branch channels to biofluid behavior and searching an improved design with optimal separation performance. It is found that changing relative lengths of branch channels is effective to both uniformity of flow rate ratio among bifurcations and reduction of difference of the flow velocities between the branch channels, whereas extending the length of the main channel from bifurcation region is only effective for uniformity of flow rate ratio.

Introduction

Microfluidics has become an important approach for designing and improving functions and performances of microdevices. As a typical application in healthcare field, the microfluidic device built with microchannels is showing increased application in biological and clinic areas. As a result of the development, Computational Fluid Dynamics (CFD) is being extensively involved and playing a very important role in gaining a better understanding microfluidic devices and their design via simulations.

An important use of microfluidic devices is for biological applications in blood separation. Traditionally, human blood is separated by large volume centrifugation where inertial forces tend to play a dominant role [1]. This approach is however not so effective in microsystem devices. This has lead to an interest in adopting new microscopic separation methods, in which viscous forces, shear strain rate, surface tension and the geometrical effects of microchannels play important roles.

The separation methods using mechanical effects may be classified into two categories: micro filter devices [2, 3] and microchannel devices [4, 5]. Among the latter, channel constriction [6, 7], bending channel [8, 9] and bifurcated channels [10, 11] have been explored. T-shaped microchannels [12, 13] have been created to produce a series of separation paths of blood cells at multiple bifurcations. The resulting device consists of a main channel and a series of perpendicularly positioned branch channels. When the flow rate ratio between the main and branch channels reaches a critical level, plasma is separated into the branch channels at a high concentration.

The important phenomena for biofluid behavior in microchannels have been expounded by several famous effects, including Fahraeus effect and Fahraeus-Lindqvist effect [14], Zweifach-Fung bifurcation effect [15, 16] and the so-called cell-free or liquid-skimming layer phenomenon. The Fahraeus effect and Fahraeus-Lindqvist effect are strongly correlated, related to the effect of changing channel cross-sections, such as a constriction, to flow hematocrit and viscosity. It was observed [17] that in a channel of 20μm diameter (this is the channel size in this study) the viscosity were only about 50% of its normal value. The cell-free layer phenomenon is a deduction from the above two effects, referring to the existence of a cell-free layer close to channel wall. With laminar flow, this separated solution may be extracted by appropriate designed apertures or branches. The Zweifach-Fung effect concerns cell behavior at bifurcations, stating that particles have a tendency to travel through the channels with higher flow rate ratio. It was observed [12] that, for a cell to channel diameter ration of the order of 1, when flow rate ratio reaches 6:1-8:1, nearly all cells will travel through the channel with the higher flow rate, leaving almost no cells travelling into the slower flow rate channel.

The geometric characteristics and boundary condition have strongly effect on the biofluid behavior in microchannels. Microchannels have two geometric characteristics: high surface-to-volume ratio and high aspect ratio of length to cross section area. These lead to boundary layer taking more volumetric share in microchannels. With no-slip of wall layer flow and relative long channel length, high pressure is required to drive the flow and the velocity is low. As the relative tolerance of microfabrication is several orders of magnitude lower than in macroscope [18], the surface quality and change rate of the cross-section of microchannels has a strong effect on flow performance. In addition, as flow rate ratio is a determined factor for separation performance in branched microchannel devices, boundary conditions has strongly influences on the relative pressures at bifurcations and become very important.

This paper presents an optimization of a microchannel mechanism used for blood plasma separation device by CFD simulation and fluid mechanics analysis. The separation efficiency of the device is modeled and analyzed firstly. Then, in view of the imperfection of the device, several improvement measures are investigated for an improved result.

Modeling and Analysis

Model establishment

The blood separator investigated in the paper is illustrated in Fig. 1. Blood is pumped into the inlet at the top and flows downstream. After passing a constriction, the blood enters the main channel which contains a number of branches where bifurcation occurs. Through these bifurcations, blood is separated into high concentrations of blood cells (main channel) and plasma (branch branches).

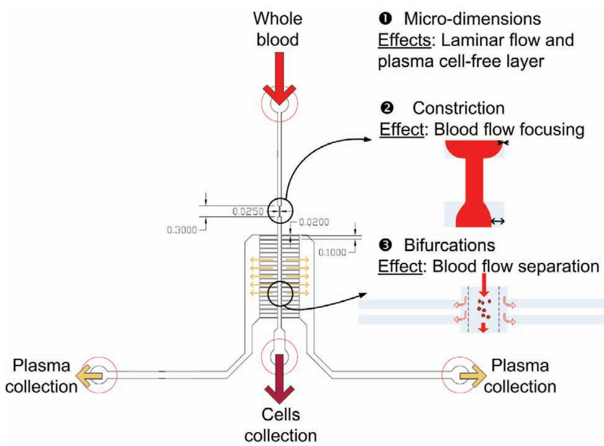

Figure 1: Blood plasma separation device. Dimensions in the figure are in millimeters [13]

The size of the device is 7mm x 10mm. The width of the main channel is 100μm. The constriction and branch side channels are 25μm and 20μm respectively. The depth of all channels is 20μm. Due to the size of the device and associated microchannel dimension, high aspect ratio of length to cross-sectional area is evident. Also evident is the high surface-to-volume ratio which will have an effect on the flow.

The analysis is based on CFD technique. The 3D finite-volume CFD package Ansys-CFX is used to perform the analysis. A thin-layer 3D model, in effect 2D, to save computer resources, is built. Figure 2 shows the computational model alongside the mesh at the first upstream bifurcation. A three-layer fine mesh is constructed in the region close to the wall to represent the flow performance in the boundary layer. In total 463,888 elements (cells) and 496,488 nodes are contained in the model. The coordinate origin is set at the left hand end of the last downstream side channel, as shown in the graphs below.

Single phase flow is used. Consequently, the constriction can be ignored. Due to the symmetric nature of the device, and assuming that the flow is symmetric, only half of the device is modeled. This consists of 15 side channels and one main channel as illustrated in Fig. 2. For the boundary conditions, the inlet is imputed a constant flow with 72μL/h (10mm/s) of flow rate. Both boundary conditions at the main and side outlets are set to 0Pa pressure.

Two models are implemented for the fluid in the main channel and branch channels, respectively, to reflect the fluid features due to separation. The fluid in the branch channels and further outcoming region in the right hand side is modeled as plasma with a constant viscosity of 0.0015 Pa s and a density of 1025kg/m^3.

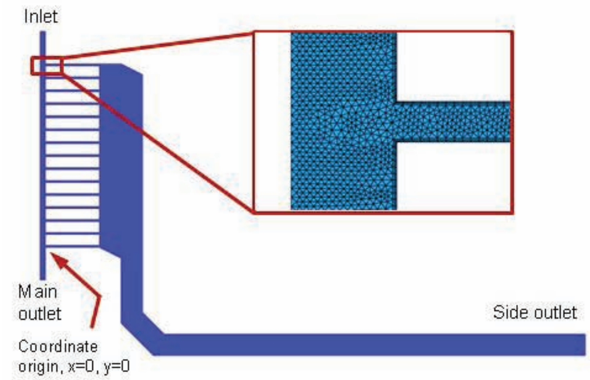

Figure 2: Computational model and the mesh in the first upstream bifurcation

The flow in the main channel is modeled as a shear rate dependent non-Newtonian flow. The Carreau-Yasuda model [19] is used for modeling the shear-thinning behavior of the fluid, shown as follow:

$$\mu(\dot{\gamma}) = \mu_\infty + \frac{\mu_0 - \mu_\infty}{(1 + (\lambda \dot{\gamma})^b)^a} \tag{1}$$

where, $\dot{\gamma}$ is the shear rate, μ_0 and μ_∞ are the infinite shear viscosity and the zero shear viscosity, respectively, λ, a and b are constants. Parameter values are as follows [19, 20]: μ_∞ = 0.0035 Pa s, μ_0 = 0.16 Pa s, λ =8.2 s, a = 1.23 and b = 0.64. The fluid density is taken as ρ = 1060kg/m^3.

Simulation result of the initial design (Case 1)

Case 1 denotes the initial design of the device. Figure 3 shows the velocity profile over the half of main channel at various bifurcations. The profile is parabolic, being zero on the channel wall and achieving the maximum velocity at the channel centre. With the parabolic distribution of velocity, cells located close to channel wall will experience a higher velocity gradient in the lateral direction towards the channel centre. Higher shear strain rate and lower viscosity are produced correspondingly in the region close to the channel wall.

Figure 4 shows the pressure development at the two ends of branch channels. The pressure difference between the two ends of the side channels reduces nearly linearly as the fluid flows in the main channel downstream from the inlet to the outlets. Figure 5 shows the velocity of the flow in the branch channels. Like the pressure difference in the branch channels, the velocities show a near linear reduction as the biofluid flows downstream. This leads to a low velocity, or low flow rate, in the last downstream channels.

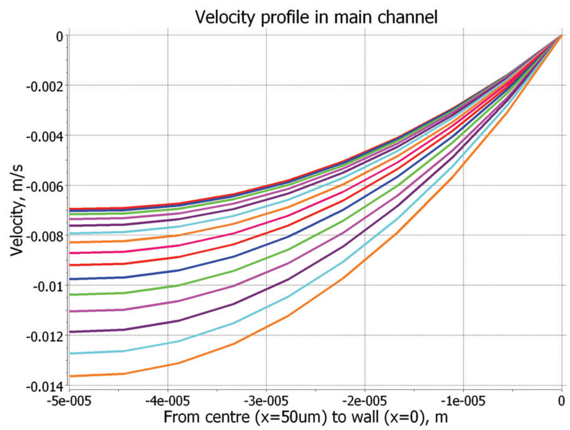

Figure 3: Flow velocities at different bifurcations in the main channel (Upstream bifurcations located on the bottom region)

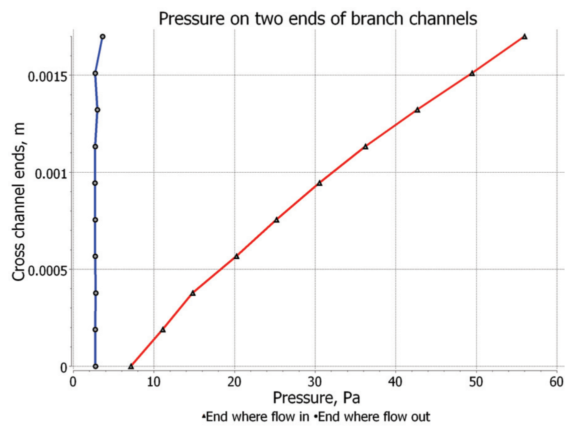

Figure 4: Pressure of the flow in two ends of the microchannels, Case 1 (The triangle symbol denotes the channel end where flow in)

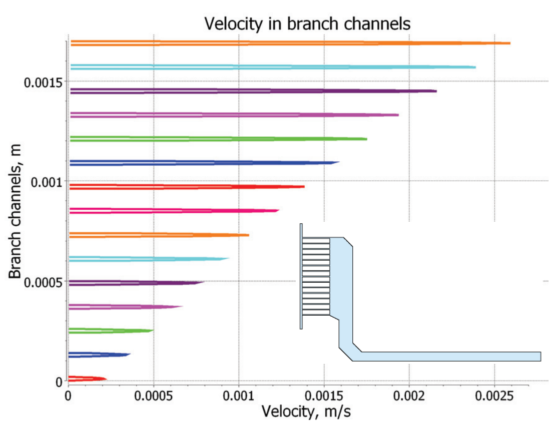

Figure 5: Flow velocities of side channels, Case 1 (Upstream channels located on the top region)

The flow rate ratio, at each bifurcation, is the ratio of the flow rate in the main channel to that in the branch channel. Table 1 shows the flow rate ratio at the bifurcations. All cases are included for comparison as explained below. The flow rate ratios of the Case 1 at all bifurcations are larger than the required 8:1 ratio. This shows that the initial design (Case 1) can separate red blood cells from plasma. However, the flow rate ratios are very different among different bifurcations, indicating the separation efficiencies will not be equal for the different branch channels. Modification of the device is required for better separation efficiency.

Table 1 Flow rate ratios at bifurcations for all cases (No 1 refers the most upstream bifurcation)

Bifurcation Number	Calculation Case			
	Case 1	Case 2	Case 3	Case 4
1	13.14	13.03	11.04	14.04
2	13.32	13.32	11.24	13.87
3	13.73	13.36	11.13	13.75
4	14.26	14.01	11.08	13.65
5	14.82	14.64	11.07	13.48
6	15.69	15.48	11.04	13.32
7	16.60	16.30	11.02	13.18
8	17.84	17.61	11.01	13.10
9	19.56	19.20	11.00	12.69
10	21.91	21.21	10.97	12.82
11	25.15	24.30	11.00	13.22
12	29.85	28.52	11.04	14.20
13	37.47			
14	51.30			
15	82.99			

Effect of Device Geometry and Design Optimization

Feature analysis of the device

From the point of fluid mechanics of view, this device (Fig. 1) has two features. (i) Comparably the outlet of the main channel is much closer to the bifurcation region than the side outlets and the width of the main channel is five times of that of the branch channel. This feature determines resistance of the branch channels is far higher than the main channel. (ii) While the channel resistance in the branch routes, including branch channels and plasma region, are nearly the same among different bifurcations, the resistance in the main channel largely vary. The resistance of the main channel from downstream bifurcations to the main outlet is much lower than the upstream bifurcations.

The first feature is concerned with the difference of the resistance between the main and branch channels. It ensures an appropriate level of flow rate ratio required for separation. The second feature is regarding to the comparison of the difference of the resistance within a channel route, either the main channel or branch routes. It causes an imbalance performance of the fluid among bifurcations (Fig. 6 and Table 1 on Case 1).

The imbalanced phenomenon is analyzed as follows. For a fully developed laminar flow, the pressure gradient shows linear distribution along channel axial direction. At bifurcation i, we have

$$Q_m^{(i)} = P^{(i)} / R_m^{(i)}(l_m, A_m, \mu_m) \tag{2a}$$

$$Q_s^{(i)} = P^{(i)} / R_s^{(i)}(l_s, A_s, \mu_s) \tag{2b}$$

where Q denotes the flow rate, P the pressure and R channel resistance. Suffixes i, m and s represent the bifurcation, the main and branch channels, respectively. Resistance R is a function of channel length l, channel cross-section area A and viscosity μ. Based on Poiseuille's law, R is directly proportional to channel length l and the viscosity μ. For a circular channel R is also inversely proportional to the fourth power of channel diameter, or the square of cross-section area. From Eq. (2), one has

$$\lambda^{(i)} = \frac{Q_m^{(i)}}{Q_s^{(i)}} = \frac{R_s^{(i)}}{R_m^{(i)}} \propto \frac{l_s^{(i)} \mu_s}{l_m^{(i)} \mu_m} \left(\frac{A_m}{A_s}\right)^2 \qquad (3)$$

where λ is the flow rate ratio of the main channel over branch channel. The area item in Eq. (3) is only valid to circular channels. Examining the geometry of the device (Fig. 1) based on Eq. (3), high flow rate ratio can be formed at bifurcations.

With identical branch channels and spacious sized plasma region (Fig. 1), the resistance between different branch routes is similar. With a series of connection, the resistance of the main channel of bifurcations is gradually reduced with the flow going downstream. From

$$l_s^{(1)} \approx l_s^{(2)} \approx l_s^{(3)} \approx \cdots \approx l_s^{(15)} \qquad (4a)$$

$$l_m^{(1)} > l_m^{(2)} > l_m^{(3)} > \cdots > l_m^{(15)} \qquad (4b)$$

one has,

$$R_s^{(1)} \approx R_s^{(2)} \approx R_s^{(3)} \approx \cdots \approx R_s^{(15)} \qquad (5a)$$

$$R_m^{(1)} > R_m^{(2)} > R_m^{(3)} > \cdots > R_m^{(15)} \qquad (5b)$$

Substituted into Eq. (3), one has,

$$\lambda^{(1)} < \lambda^{(2)} < \lambda^{(3)} < \cdots < \lambda^{(15)} \qquad (6)$$

Eq. (6) is evident by Table 1 on Case 1.

There are two measures to rectify the imbalance. One is from the main channel: moving the bifurcation region leaving from the outlet of the main channel, so that the differences of resistance among bifurcations become indistinct. The other measure is targeted at branch channels: changing the resistance of branch route according to the resistant changing rate of the main channel, so that both the main channel and branch routes have declined resistance changing rates from upstream to downstream bifurcations. Implemented into the device, the first measure means an extension of the main channel from bifurcation region. The second measure requires channel resistance of the branch channels to be gradually reduced, by gradually decreasing channel lengths or gradually increasing channel cross-section areas.

Apart from the above two features, there is another detail of the design that may affect flow distribution. There is a terrace (Fig. 1 or 2) located at the outlet end of the last downstream channel. The flow outcoming from upstream channels may form a certain pressure at the right hand end of the last downstream branch channel by the terrace.

Summarizing above, improvements can come from three ways: (i) lowering the terrace from the outlet end of the last downstream channel; (ii) extending the length of the main channel; (iii) gradually reducing the resistance of the branch channels from upstream to downstream channels. These three solutions will be investigated below with regard to Cases 2, 3 and 4.

A local improvement (Case 2)

Case 2 refers to a simple modification, in which the last three branch channels are blocked/removed. This leads to the effectiveness of extension of the main channel from bifurcation region and moving down the terrace from the outlet end of the last downstream branch channel. With this change, the number of branch channels is reduced to 12 from 15. The geometry of Case 2 is included in Fig. 6.

Figure 6 shows the flow velocity of the branch channels. Figure 7 shows the flow velocity at bifurcations in the main channel. The flow rate ratios of bifurcations are shown in Table 1. Compared with Cases 1 (Fig. 3), the velocity and flow rate ratio of the 12 channel mechanism (Case 2) is nearly the same as the first 12 channels of the 15 channel mechanism (Case 1). This fact implies that, with a fixed length of the main channel, the flow velocity of branch channels and flow rate ratio at bifurcations are mainly determined by the relative positions of branch channels coupled on the main channel. Therefore, shifting branch channels along the main channel can vary velocity and flow rate ratio of branch channels but the velocity difference between branch channels cannot be changed.

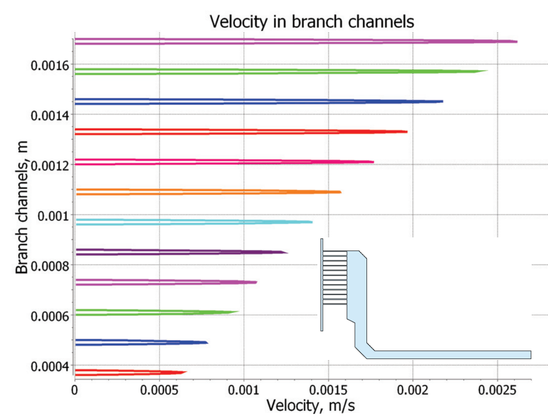

Figure 6: Flow velocities of branch channels, Case 2 (Upstream channels located on the top region)

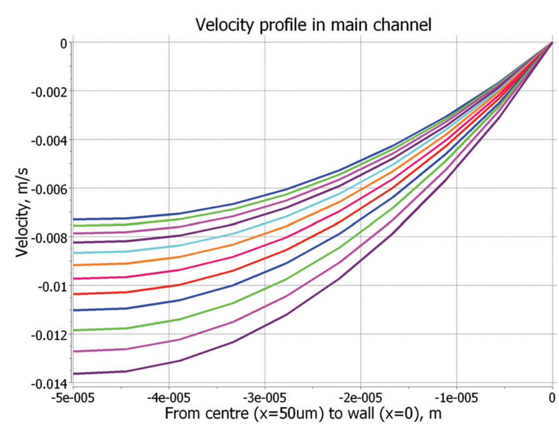

Figure 7: Flow velocities at different bifurcations in the main channel (Upstream bifurcations located on the bottom region)

The optimization in the following two subsections will be based on this 12 channel mechanism. The objective of the optimization is a uniform flow rate ratio, representing uniform separation efficiency among different bifurcations.

Effect of the length of the main channel length on separation efficiency (Case 3)

The effect of extending main channel on flow rate ratio distribution is investigated in Case 3. In Case 3, a series of simulations have been carried out, in which the main channel is extended by different lengths from bifurcation region. The extension distance is counted from the origin point of y coordinate (Fig. 2). The channel extension length ranges from 0.1mm to 1.3mm is steps of 0.2mm. Case 2 represents the geometry when the main channel is extended by 0.3mm. Figure 8 shows the variation of the flow rate ratios on bifurcations 1, 4, 7, 10 and 12 as a function of the extension length of the main channel. The extension length shows a strong effect on the flow rate ratio, especially for downstream bifurcations. The flow rate ratios among different bifurcations vary largely for a short extension and gradually tend towards the same level with the increase of the extension length of the main channel. A uniform flow rate ratio is achieved when the main channel is extended by 1.2mm, shown in Table 1. This means that the separation efficiency becomes constant across the channels as the bifurcation region moves into relative upstream region of the main channel and thus the difference of pressure and resistance between bifurcations is lightened over the increased whole region.

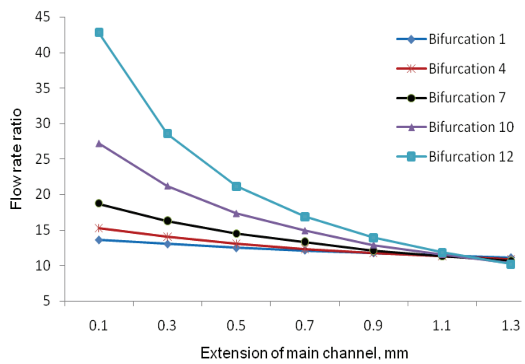

Figure 8: Flow rate ratio against extension distance of main channel at bifurcations 1, 4, 7, 10 and 12 (No 1 refers the most upstream bifurcation)

Figure 9 shows the velocity of flow in the branch channels when the main channel is extended by 1.2mm. Compared with the Case 2 (Fig. 6), the velocity of the flow is largely increased due to the increased distance, i.e. pressure, from bifurcation region to the main outlet. However, the difference of flow velocity among the channels is little changed. This is because the imbalance among bifurcations on the resistance of the main channel and branch routes still exists.

Figure 10 shows the velocity of the main channel at different bifurcations. Compared with Case 1 (Fig. 3), the velocity difference at each bifurcation gradually increases when the flow goes downstream, implying an increase of fluid flowing through the downstream side channels. Whereas the extension of the main channel increases the flow velocity and pressure drop at the branch channels, the difference in the flow velocity between the branch channels is unaffected.

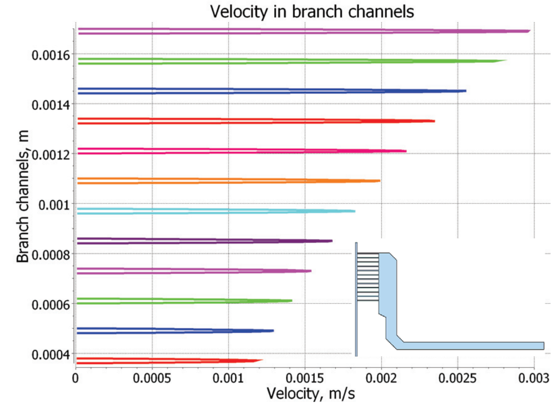

Figure 9: Flow velocities of branch channels, Case 3 (Upstream channels located on the top region)

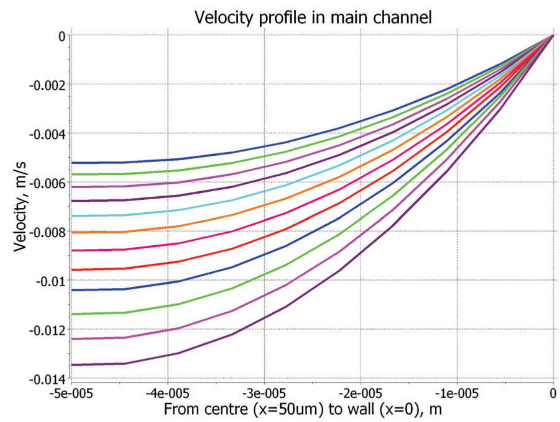

Figure 10: Flow velocities at bifurcations in the main channel, Case 3 (Upstream bifurcations located on the bottom region)

Effect of the geometry of branch channels on separation efficiency (Case 4)

Case 4 investigates the effect of changing geometry of the branch channels on flow rate ratio. In all the above cases, Cases 1 to 3, the velocity of branch channels from the upstream to downstream shows linear reduction. This is because equal length branch channels have a similar resistance from the bifurcation region to side outlet, whereas the resistance in main channel is different among bifurcations. This situation can be modified by gradually reducing the resistance of branch channels from upstream to downstream.

Channel length of the branch channels is chosen as the variable. It is assumed that the optimal geometry of the branch channels show linear length reduction from upstream to downstream channels. In the searching process for an improved solution, the length of the most upstream branch channel is fixed at 0.6mm. The last downstream channel is simulated by a series of lengths, ranging from 0.1mm to 0.4mm is steps of 0.05mm. The length of the branch channels between the most upstream and the last downstream channels is set to a linear reduction and evenly fitted from the top to bottom. Figure 11 shows the variation of the flow rate ratios on bifurcations 1, 4, 7, 10 and 12 as a function of the channel length of the last downstream branch channel.

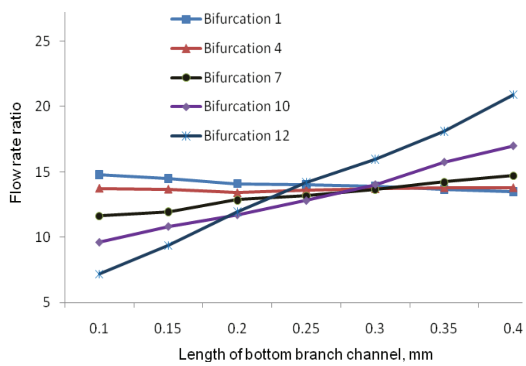

Figure 11: Flow rate ratio against extension distance of main channel at bifurcations 1, 4, 7, 10 and 12 (No 1 refers the most upstream bifurcation)

Comparing Fig. 11 with Fig. 8, a distinct difference between Case 4 and Case 3 is the development pattern of flow rate ratio. In Case 3, with the increase of the extension distance of the main channel, the scattered flow rate ratios at different bifurcations gradually converged to a fixed data. This shows that the process is stable and convergent. This implies that, with the bifurcation region moving far away from the main outlet, relatively the effect of the difference of pressures between bifurcations become small and trivial. In contrast, in Case 4, the flow rate ratios at bifurcations develop along straight lines. The slopes of lines are different, being flat for the most upstream bifurcations and becoming more inclination with the increase of the bifurcation number. This shows that the flow rate ratio of downstream bifurcations is strongly affected by the change of geometry of the branch channels.

It can be seen from Fig. 11 that the straight lines of flow rate ratios at different bifurcation do not cross at the same point. The lines of most channels cross at 0.3mm, the half of the length of the most upstream channel, but the last bifurcation (bifurcation 12) shifts from the point. At 0.25mm, flow rate ratios are located in a small range, but not cross with each other, shown in Table 1.

Figure 12 shows the velocity of branch channels when the length of the last downstream channel is 0.25mm. Similar as Cases 2 and 3 (Fig. 6 and 9), the velocity of different branch channels shows linear distribution. However, the velocity differences between bifurcations become smaller than the former cases. This indicates that changing the geometry of the branch channels have effect on reducing the difference of velocities between branch channels.

Figure 13 shows the flow velocity of branch channels with the length of the last downstream channel reduced to 0.15mm. The effect of changing geometry of the branch channels on the velocity of the channels can be clearly viewed. Compared with Fig. 12, the velocity difference between the branch channels becomes smaller. Hence, changing geometry of the branch channels is effective on both uniformity of flow rate ratio and reduction of velocity difference of the branch channels among bifurcations.

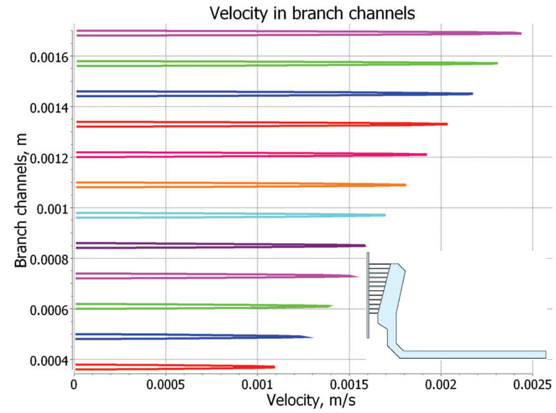

Figure 12: Flow velocities of branch channels, Case 3 (Upstream channels located on the top region)

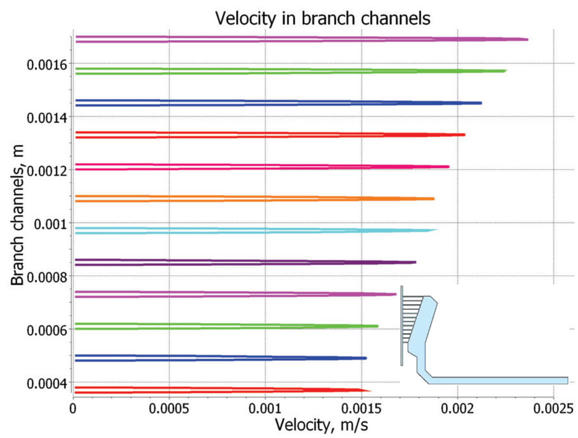

Figure 13: Flow velocities of branch channels, with the length of the last downstream channel by 0.15mm (Upstream channels located on the top region)

Conclusions

Biofluid behavior in a T-microchannel device is investigated and design optimization for better performance in terms of particle separation is carried out. Single phase shear rate non-Newtonian flow is used in modelling. The performance of separation of blood cells from plasma is evident with various effects, such as Zweifach-Fung bifurcation law, Fahraeus effect, Fahraeus-Lindqvist effect and cell-free phenomenon. Although not simulating blood cells explicitly, this approach has provided a unique insight into the flow behavior.

This device shows ability for blood plasma separation. However, the separation efficiency varies among different bifurcations. The imperfection of the device is analyzed with fluid mechanics. It is found that T-microchannel device with equal length of branch channels cannot lead to uniform velocity among branch channels and, if the outlet of the main channel is close to the bifurcation region, flow rate ratio will show large variations among bifurcations. The reason is that while equal length branch channels produce a similar resistance from each bifurcation through a branch route, the resistance of the main channel from bifurcations may be very different. Therefore, at different bifurcations, the resistance rate between the branch route and the main channel route is generally different.

Two improvement approaches are investigated by numerical iteration searching and optimization. One is concerned with the main channel. The length of the main channel is extended from its outlet, so that the difference of the resistance or pressure between bifurcations is relatively reduced. The other is targeted at the branch channels. The lengths of the branch channels are changed with a constant rate to form a linear reduction from upstream to downstream branch channels to mimic the resistance change pattern at bifurcations in the main channel.

The length of the main channel from bifurcation region has a strong effect to flow rate ratio. A short length can reduce channel resistance and result in high flow rate ratio, but flow rate ratio may largely vary due to the large relative difference of resistance among bifurcation. A long length can lead to uniformity of flow rate ratio among bifurcations but, with the increase of channel resistance, the value of flow rate ratio becomes lower. The simulation shows that the extension of the main channel leads to a uniform flow rate ratio among bifurcations, implying a balanced separation from bifurcations. The difference between the velocities of the branch channels remains the same as the initial, indicating the imbalanced resistance between the main and branch routes still exists. The change of geometry of the branch channels is effective for both improvement of flow rate ratio and branch channel velocity, implying this can lead both the resistances of the main and branch routes to be reduced simultaneously with the increase of bifurcations.

Acknowledgments

The authors gratefully acknowledge the financial support by the UK Engineering and Physical Sciences Research Council (EPSRC) in funding the Grand Challenge Project '3D-Mintegration' (www.3D-mintegration.com), referenced EP/C534212/1, and the financial support from the Scottish Funding Council (SFC) through the Scottish Consortium in MicroPhotonic Systems (SCIMPS). The authors would also like to acknowledge their gratefulness to the inspired discussions and suggestions offered by David Topham.

References

1. Hester, J.P., Kellogg, R.M., Mulzet, A.P., Kruger, V.R., McCredie, K.B., Freireich, E.J., "Principles of blood separation and component extraction in a disposable continuous-flow single-stage channel," *Blood,* Vol. 54 (1979), pp. 254-68.
2. Carlson, R., Gabel, C., Chan, S., Austin, R., "Self-sorting of white blood cells in a lattice," *Phys. Rev. Lett*. Vol. 79 (1997), pp. 2149–2152.
3. Wilding, P., Kricka, L.J., Cheng, J., Hvichia, G., Shoffner, M.A., Fortina, P., "Integrated cell isolation and polymerase chain reaction analysis using silicon microfilter chambers," *Anal. Biochem*. Vol. 257 (1998), pp. 95–100.
4. Mohamed, H., Turner, J.N., Caggana, M., "Biochip for separating fetal cells from maternal circulation," *Journal of Chromatography A,* Vol. 1162 (2007), pp. 187-192.
5. Rainer, J., Roger, S., Carlo, E., "Microfluidic depletion of red blood cells from whole blood in high-aspect-ratio microchannels," *Microfluid Nanofluid*, Vol. 3 (2007), pp. 47-53.
6. Layek, G.C., Midya, C., "Effect of constriction height on flow separation in a two-dimensional channel," *Commun Nonlinear Sci Numer Simul*, Vol.12 (2007), pp.745–759.
7. Midva, C., Layek, G.C., Gupta, A.S., Mahapatra, T.R., "Magnetohydrodynamic Viscous Flow Separation in a Channel with Constrictions," *J. Fluids Eng*. Vol. 125 (2003), pp. 952-962.
8. Blattert, C., Jurischka, R., Tahhan, I., Schoth, A., Kerth, P., Menz, W., "Microfluidic blood/plasma separation unit based on microchannel bend structures," *Proc of microtechnology in medicine and biology*, *3rd IEEE/EMBS Special Topic Conf*, Honolulu, Hawaii, 12-15 May 2005, pp. 38-41.
9. Carlo, D.D., Edd, J.F., Irlmla, D., Tompkins, R.G., Toner, M., "Equilibrium separation and filtration of particles using differential inertial focusing," *Anal. Chem*. Vol. 80 (2008), pp. 2204-2211.
10. Pries, A.R., Secomb, T.W., Gaehtgens, P., Gross, J.F., "Blood flow in microvascular networks, experiments and simulation," *Circ Res*. Vol. 67 (1990), pp. 826-834.
11. Jafari, A., Mousavi, S.M., Kolari, P., "Numerical investigation of blood flow, Part I: in microvessel bifurcations," *Commun Nonlinear Sci Numer Simul*, Vol. 13 (2008), pp. 1615-1626.
12. Yang, S., Undar, A., Zahn, J.D., "A microfluidic device for continuous, real time blood plasma separation," *Lab Chip*, Vol. 6 (2006), pp. 871-880.
13. Kersaudy-Kerhoas, M., Kavanagh, D, Xue X., Patel M.K., Dhariwal R., Bailey C., Desmulliez M.P.Y., "Integrated biomedical device for flood preparation," *Proc of ESTC conf*, London, 1-4 September 2008, pp. 447-452.
14. Brown, B.H. *et al*, Medical Physics and Biomedical Engineering. Institute of Physics Publishing (Bristol, 1999)
15. Svanes, K., Zweifach, B.W., "Variations in small blood vessel hematocrit produced in hypothermic rats by micro-occlusion," *Microvasc Res*, Vol. 1 (1968), pp. 210-220.
16. Fung, Y.C. (1973) "Stochastic flow in capillary blood vessels," *Microvasc. Res*. Vol. 5 (1973), pp. 34-48.
17. Woodcock, J.P., "Physical properties of blood and their influence on blood-flow measurement," *Rep. Prog. Phys*. Vol. 39 (1976), pp. 65-127.
18. Madou, Marc J., Fundamentals of Microfabrication, the Science of Miniaturization, 2nd ed, CRC Press LLC (London, 2002).
19. Leuprecht, A. and Perktold, K., "Computer simulation of non-newtonian effects on blood flow in large arteries," *Comput. Methods Biomech. Biomed. Eng*., Vol. 4 (2001), pp. 149-163.
20. Abraham, F., Behr, M. and Heinkenschloss, M., "Shape optimization in steady blood flow: A numerical study of non-Newtonian effects," *Comput. Methods Biomech. Biomed. Eng*., Vol. 8, No. 2 (2005), pp. 127-137.